

# Structural Phase Diagram of $\text{Ca}_{1-x}\text{Y}_x\text{MnO}_3$ : Characterization of Phases

D. Vega, G. Polla, A. G. Leyva, P. König, H. Lanza, and A. Esteban

*Centro Atómico Constituyentes, Comisión Nacional de Energía Atómica, Avda. del Libertador 8250, 1429 Buenos Aires, Argentina*

and

H. Aliaga, M. T. Causa, M. Tovar, and B. Alascio

*Centro Atómico Bariloche and Instituto Balseiro, Comisión Nacional de Energía Atómica and Universidad Nacional de Cuyo, 8400 San Carlos de Bariloche, Argentina*

Received June 29, 2000; in revised form October 12, 2000; accepted November 6, 2000

To help the understanding of the physical behavior of  $\text{Ca}_{1-x}\text{Y}_x\text{MnO}_3$ , its phase diagram in the whole  $x$  concentration range was investigated taking into account the stability of phases and the possible coexistence of different structural phases. By careful analysis of powder X-ray diffraction (XRD) patterns, we were able to observe the following phase diagram: (i) Orthorhombic phases were detected both in the region of  $0 \leq x \leq 0.25$  (O type phase with Ca site twelve fold coordinated) and in the region of  $0.5 \leq x < 0.75$  (O' type phase with Ca site ninefold coordinated). (ii) Phase segregation for  $0.25 \leq x \leq 0.5$  and for  $x \geq 0.75$  that have not been reported previously, hexagonal  $\text{YMnO}_3$ , segregates as a separate phase for  $x > 0.75$ , and for  $0.25 \leq x \leq 0.5$  the coexistence of  $\text{Ca}_{0.75}\text{Y}_{0.25}\text{MnO}_3$  (O) and  $\text{Ca}_{0.5}\text{Y}_{0.5}\text{MnO}_3$  (O') have to be included in the refinement for it to converge. © 2001 Academic Press

**Key Words:** oxomanganates; manganites; phase diagram; structural characterization.

## INTRODUCTION

The mixed oxides of general formula  $A\text{MnO}_3$ , where  $A$  is an alkaline-earth ion, belong to the group of orthorhombic distorted perovskites. Within these compounds,  $\text{CaMnO}_3$  crystallizes in space group  $Pnma$  with  $a = 5.279$  Å,  $b = 7.448$  Å, and  $c = 5.264$  Å. The  $\text{Mn}^{4+}$  has an octahedral oxygen coordination environment with an axial oxygen ( $\text{O}_1$ ) and two equatorial ones ( $\text{O}_2$  and  $\text{O}_{22}$ ).  $\text{Ca}^{2+}$  occupies the center of a distorted dodecahedron of oxygens. The substitution of bivalent cations by trivalent ones leads to the simultaneous occurrence of  $\text{Mn}^{3+}$  and  $\text{Mn}^{4+}$  ions in the crystalline structure and significantly modifies the structural and transport properties presenting complex phase diagrams including phases with different magnetic and charge order. Important magnetoresistance (MR) effects, asso-

ciated to the multivalent state of the Mn ions, were found. The MR is believed to be the result of ferromagnetic (FM) double-exchange (DE) interactions between  $t_{2g}$  electrons mediated by itinerant spin polarized  $e_g$  electrons (3).

Recently, technological interest regarding yttrium-doped-calcium manganate arose since can be used as an oxygen electrode for a solid oxide fuel cell. The system  $\text{Ca}_{1-x}\text{Y}_x\text{MnO}_3$  has been extensively discussed recently (5–9), showing some discrepancies such as those evident in the following papers: in (8) a solid solution is found in the range of  $0 = x < 0.75$  and segregation of  $\text{YMnO}_3$  for  $x > 0.75$ . This segregation was also found in (4) for  $x > 0.78$ , on the other hand, in (9) a complete solid solution is found for the composition range  $0.4 \leq x \leq 1$  without any segregation and a phase transition for  $x = 0.78$ .

$\text{YMnO}_3$  crystallizes in the  $P6_3cm$  hexagonal space group with  $a = 6.12$  Å and  $c = 11.39$  Å. The two independent  $\text{Y}^{3+}$  ions are coordinated by seven oxygen atoms, while the only  $\text{Mn}^{3+}$  is pentacoordinated by oxygen atoms (10).

In this work we have examined the effect of yttrium doping for the whole  $x$  concentration range in the structural properties of the  $\text{CaMnO}_3$  perovskite compound. This particular doping introduces a significant mismatch between the cations radii as yttrium is much smaller than calcium. The relationship between structural, transport and magnetic properties is discussed.

## EXPERIMENTAL

Ceramic samples of the  $\text{Ca}_{1-x}\text{Y}_x\text{MnO}_3$  system with  $0 \leq x \leq 1$  were synthesized through a solid-state reaction starting from stoichiometric proportions of  $\text{CaCO}_3$ ,  $\text{Y}_2\text{O}_3$ , and  $\text{MnCO}_3$  reactants whose purity had been checked previously. The powders were ground, mixed together, and heated in air up to  $1400^\circ\text{C}$  for 15 hs and then furnace cooled

down to room temperature at a rate of  $100^\circ\text{C}/\text{h}$ . Redox titrations were used to establish the total amount of Mn and  $\text{Mn}^{4+}$  in several samples (11).

Powder X-ray diffraction patterns were taken at ambient temperature for phase identification and for Rietveld refinement using a Philips PW 3710 diffractometer with Cu graphite monochromatized radiation, with a  $1/2^\circ$  scattering slit and a  $2\theta$  step of  $0.02^\circ$ . Rietveld refinement was performed with the FullProf code (12) and with isotropic displacement conditions.

Electrical resistivity ( $\rho$ ) was measured with the four-probe method and magnetization ( $M$ ) with a SQUID magnetometer, both  $\rho$  and  $M$  in the temperature range 5–300 K.

## RESULTS

In Table 1 we show the redox titration values obtained for the total amount of Mn and  $\text{Mn}^{4+}$  as a function of the Y doping. By comparison with the nominal values corresponding to each sample it can be seen that for  $0.0 \leq x \leq 0.25$  all the samples are slightly oxygen deficient, while for  $0.5 \leq x < 0.75$  the samples are stoichiometric. This is in accordance with the observations in the manganates  $\text{Ca}_{1-x}\text{La}_x\text{MnO}_3$ . In this case, for highly doped samples ( $x = 0.67$ ), it has been shown (13) that the oxygen content remains unchanged, at 3.000 (2), while the oxygen partial pressure,  $P(\text{O}_2)$ , varied between 1 atm and  $10^{-4}$  atm. For samples near  $x = 0$ , similar variations in  $P(\text{O}_2)$  change the

**TABLE 1**  
 **$\text{Ca}_{1-x}\text{Y}_x\text{MnO}_3$  Samples, Nominal Yttrium Concentration, Measured  $\text{Mn}^{4+}$  Weight Percentage and Percentage of Each  $\text{Ca}_{1-x}\text{Y}_x\text{MnO}_3$  Phases**

$x$	$\text{Mn}^{4+}$ (w%) $\pm 2\%$	Oxygen content	$\text{Ca}_{1-x}\text{Y}_x\text{MnO}_3$ (%) $\pm 2$
0.00	93	2.97	100% O phase
0.10	84	2.97	100% O phase
0.20	75	2.97	100% O phase
0.25	—	—	100% O phase
0.30	—	—	76% O phase $x = 0.75$ + 24% O' phase $x = 0.50$
0.35	—	—	52% O phase $x = 0.75$ + 48% O' phase $x = 0.50$
0.40	—	—	25% O phase $x = 0.75$ + 75% O' phase $x = 0.50$
0.50	48	2.99	100% O' phase
0.60	39	3.00	100% O' phase
0.67	33	3.00	100% O' phase
0.75	26	3.00	97% O' phase + 3% $\text{YMnO}_3$ (Hex)
0.80	—	—	90% O' phase + 10% $\text{YMnO}_3$ (Hex)
0.90	—	—	59% O' phase + 41% $\text{YMnO}_3$ (Hex)
0.95	—	—	79% O' phase + 21% $\text{YMnO}_3$ (Hex)
1.00	0	3.00	100% $\text{YMnO}_3$ (Hex)

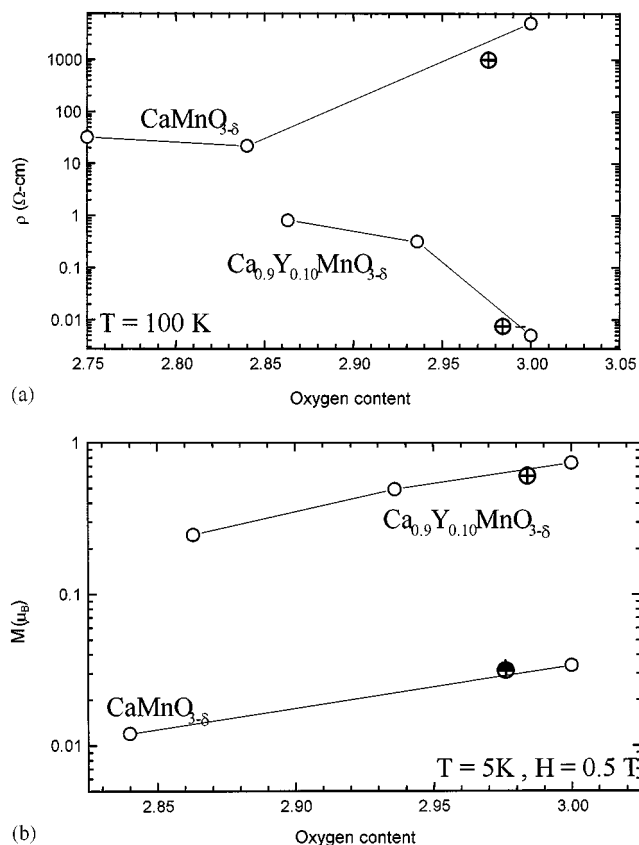


**FIG. 1.** (a)  $\rho$  vs  $\delta$  measured at 100 K. (b)  $M$  vs  $\delta$  measured at 5 K with an applied magnetic field  $H = 0.5$  T. Open symbols, data from Refs. (14) and (15). Crossed symbols, this work.

oxygen content from 3.00 to 2.66 (14). In order to evaluate the effects of the nonstoichiometry on the physical properties we compare, in Figs. 1a and 1b our measurements for  $\rho$  and  $M$  with previous results (14,15) on the series  $\text{CaMnO}_{3-\delta}$  and  $\text{Ca}_{0.9}\text{Y}_{0.1}\text{MnO}_{3-\delta}$  where the oxygen content,  $\delta$ , was carefully controlled by thermogravimetric methods. The measured  $M$  and  $\rho$  for  $x = 0$  and 0.10 in our samples are very close to the stoichiometric case. Besides, the small differences observed are in agreement with the dependence of  $\rho(\delta)$  and  $M(\delta)$  measured in a larger  $\delta$  range (see Fig. 1).

XRD patterns for  $\text{Ca}_{1-x}\text{Y}_x\text{MnO}_3$  are shown in Fig. 2. For high yttrium concentration, hexagonal  $\text{YMnO}_3$  segregates from the yttrium saturated O' phase and it can be quantified by Rietveld refinements (Table 1). The amount of hexagonal phase increases steadily from 0 to 100% from  $x = 0.75$  to  $x = 1$ . No changes on the lattice parameters of the hexagonal phase were found, revealing that under these synthesis conditions no calcium is incorporated in this phase. Occupancy factors of the Y/Ca site obtained from Rietveld refinement confirm that the solubility limit of the yttrium content is about 0.75. The  $\text{Ca}_{0.25}\text{Y}_{0.75}\text{MnO}_3$

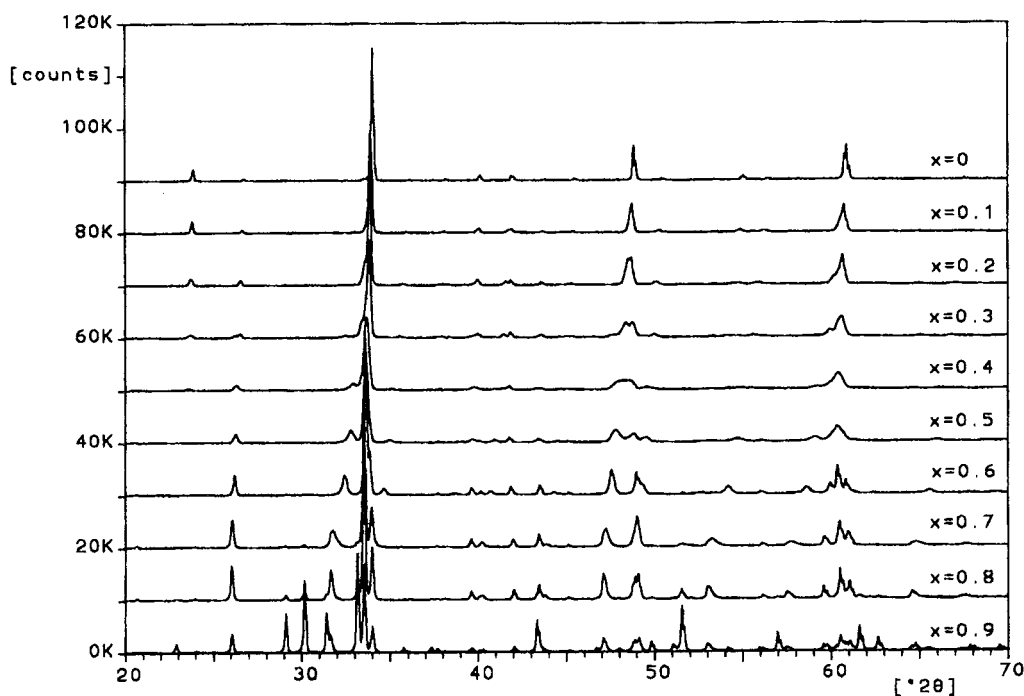


FIG. 2. XRD patterns for samples  $\text{Ca}_{1-x}\text{Y}_x\text{MnO}_3$ .

orthorhombic phase coexists with the hexagonal  $\text{YMnO}_3$  phase in this range.

Rietveld refinements allowed us to distinguish three different regions in the structural phase diagram:

- For low yttrium concentration,  $0.0 \leq x \leq 0.25$  from Rietveld refinement the orthorhombic O-phase was obtained with  $c < b/\sqrt{2} < a$ . A typical refinement for the  $\text{Ca}_{0.8}\text{Y}_{0.2}\text{MnO}_3$  compound with the orthorhombic O structure is shown in Fig. 3 (inset).
- For high yttrium concentrations,  $0.5 \leq x < 0.75$ , the orthorhombic O' model with  $b/\sqrt{2} < c < a$  converged to more reliable residual parameters.
- For intermediate yttrium concentrations Rietveld refinements under the conditions mentioned above lead to very high final agreement factors. For this range of  $x$  the refinement notably improves if coexistence of both O and O' phases were taken into account (see Fig. 3).

For yttrium concentration above 0.25 a new phase of composition  $\text{Ca}_{0.5}\text{Y}_{0.5}\text{MnO}_3$  (O' phase) segregates and coexists with  $\text{Ca}_{0.75}\text{Y}_{0.25}\text{MnO}_3$  phase (O phase). The pattern intensity corresponding to the  $\text{Ca}_{0.75}\text{Y}_{0.25}\text{MnO}_3$  phase diminishes while the  $\text{Ca}_{0.50}\text{Y}_{0.50}\text{MnO}_3$  phase increases as a function of increasing yttrium concentration (see Table 1), until the nominal concentration reaches  $x = 0.5$ , where a single phase is obtained. This single phase continues incorporating yttrium atoms up to  $x = 0.75$ , onward the hexagonal phase segregates, and no more yttrium is incorp-

orated in the orthorhombic phase. Phase diagram and cell parameters as a function of yttrium concentration are shown in Fig. 4a.

The  $\text{MnO}_6$  octahedron distortions and the changes in the Mn coordination distances are shown in Fig. 4b. The distortions can be described using two different angles: the "rotation angle"  $\omega$  ( $\omega = (180^\circ - [\text{Mn-O2-Mn}])/2$ ) and the "tilt angle"  $\varphi$  ( $\varphi = (180^\circ - [\text{Mn-O1-Mn}])/2$ ), Fig. 4c shows the dependence of these angles with  $x$ .

## DISCUSSION

All the samples synthesizing in the orthorhombic O-phase ( $x \leq 0.25$ ) keep Mn-O distances isometric even when the yttrium concentration increases (see Fig. 4b). The  $\text{MnO}_6$  octahedron tilts to compensate the diminishing of the mean cationic radius of the A site,  $r_A$ , and the slight increase of the Mn radii ( $r_{\text{Mn}^{3+}} > r_{\text{Mn}^{4+}}$ ) with  $x$ . Goldschmidt calculated the optimal size of the A cation from the B ionic radii by treating the lattice as a perfect close-packed one, twice the M-O bond distance is equal to the cell edge and twice A-O bond distance is equal to the length of a face diagonal. This geometric relationship is known as the Goldschmidt tolerance factor,  $t = R_A + R_O/\sqrt{2}(R_M + R_O)$ .

In the present work, the tolerance factors for all samples were calculated using the 9 coordination ionic radii since no information on 12 coordinated ionic radii is reported in the

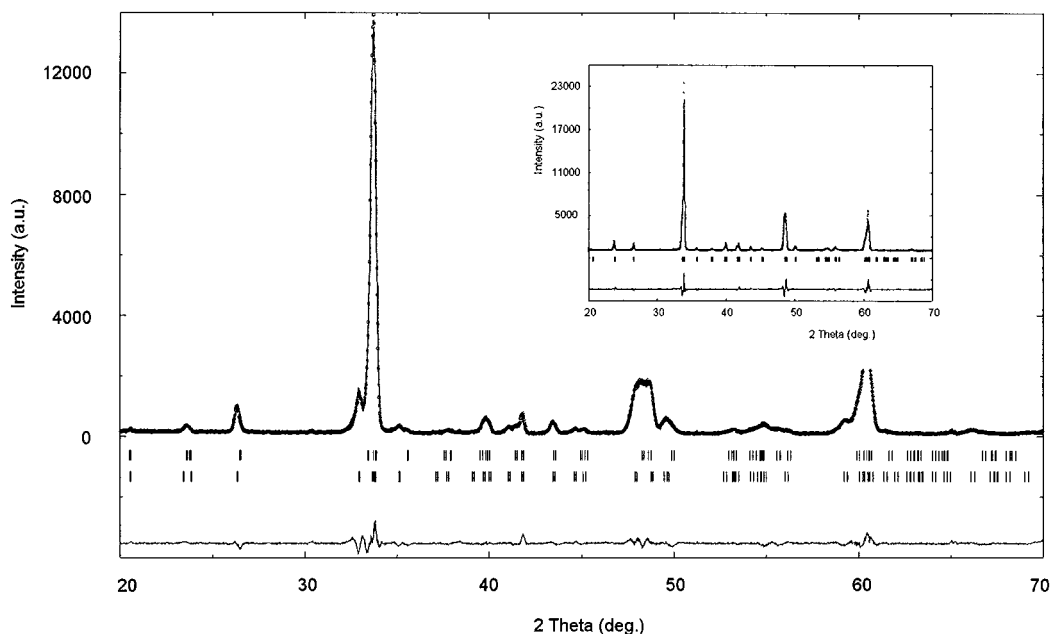


FIG. 3. Rietveld refinement of  $\text{Ca}_{0.6}\text{Y}_{0.4}\text{MnO}_3$  (Rp, 7.6; Rwp, 10.8) (Inset)  $\text{Ca}_{0.8}\text{Y}_{0.2}\text{MnO}_3$  (Rp, 10.8; Rwp, 14.4).

Shannon table for  $\text{Y}^{3+}$ ; in the  $R_M$  calculation the proportion of  $\text{Mn}^{3+}$  and  $\text{Mn}^{4+}$  is taken into account. Following the original Goldschmidt ideas, a steric factor  $s = A - O / \sqrt{2}(\text{Mn} - \text{O})$  was calculated for all samples from the mean values of  $A$ - $\text{O}$  and  $\text{Mn}$ - $\text{O}$  bond distances. For those  $\text{O}$  phases, 12  $A$ - $\text{O}$  bond distances were considered while for  $\text{O}'$  phases only 9  $A$ - $\text{O}$  bond distances were taken into account since the large tilt and rotation angles make it impossible to consider 12  $\text{O}$  ions in the first coordination sphere. As shown in Fig. 5, in the high yttrium concentration region a good agreement between the steric and the tolerance factors were obtained. A low tolerance factor is associated with high rotation and tilt angles. Nine coordination polyhedron for  $A$  cation and an increment of  $\text{Mn}$ - $\text{O}_2$  bond distances result. These distortions are compatible with a cooperative Jahn-Teller effect.

On the other hand, in the region of low yttrium concentration the steric factor is higher than the tolerance one. For steric factors around 1, there will be enough space to have a 12 coordination site for the  $A$  cation and high rotation and tilt angles are not necessary.

For  $\text{O}'$ -phase samples ( $0.5 \leq x \leq 0.75$ ), Fig. 4c shows important angular distortion, in both rotation and tilt angles.

With our synthesis condition, two different phases,  $\text{Ca}_{0.75}\text{Y}_{0.25}\text{MnO}_3$  ( $\text{O}$ ) and  $\text{Ca}_{0.5}\text{Y}_{0.5}\text{MnO}_3$  ( $\text{O}'$ ), coexist in the intermediate region ( $0.25 \leq x \leq 0.5$ ), the relative amount depends on the nominal  $x$  concentration. This result differs from those previous reports (4, 8, 9), where a solid solution was also found for this range of concentration.

In Fig. 6 we show the  $x$  dependence of  $\rho$  and  $M$  measured in our samples. Only single-phase materials were analyzed. In the region of low  $\text{Y}$  doping ( $x \leq 0.25$ ) our results are in qualitative agreement with the findings in (6) for this system and those of (18) for similar  $x$  values in  $\text{Ca}_{1-x}\text{La}_x\text{MnO}_3$ . As is seen in this figure, small yttrium substitution for  $\text{Ca}$  causes a significant decrease in  $\rho$  and increases  $M$ . At room temperature,  $\rho$  remains approximately constant for  $0 < x \leq 0.25$ . However at  $T = 100$  K the behavior is not uniform in this concentration range. For  $x \leq 0.15$ ,  $\rho(100 \text{ K}) \approx \rho(300 \text{ K})$  but an increase of several orders of magnitude in  $\rho$ , accompanied by a drop in the magnetization, is observed for  $0.15 < x \leq 0.25$ . This behavior can be explained assuming the existence of a charge-order state at  $T < 200$  K where anomalies in the  $\rho(T)$  dependence were found in (18) and (19).

For the highly distorted samples,  $x \geq 0.5$ ,  $M$  increases again. However, this behavior is not followed by a diminution in  $\rho$  (see Fig. 6), in disagreement with the observations in the  $\text{Ca}_{1-x}\text{La}_x\text{MnO}_3$  case. In the  $\text{La}$ -doped system, as in other manganates (2), a metal-insulator transition in coincidence with a FM phase and important MR effects were observed. In our case, the total ferromagnetic state with  $M > 3 \mu_B$  is never achieved.

## CONCLUSIONS

The study of physical properties of manganates, such as  $\text{Ca}_{1-x}\text{Y}_x\text{MnO}_3$ , requires single-phase samples because electrical transport and magnetic properties are closely related

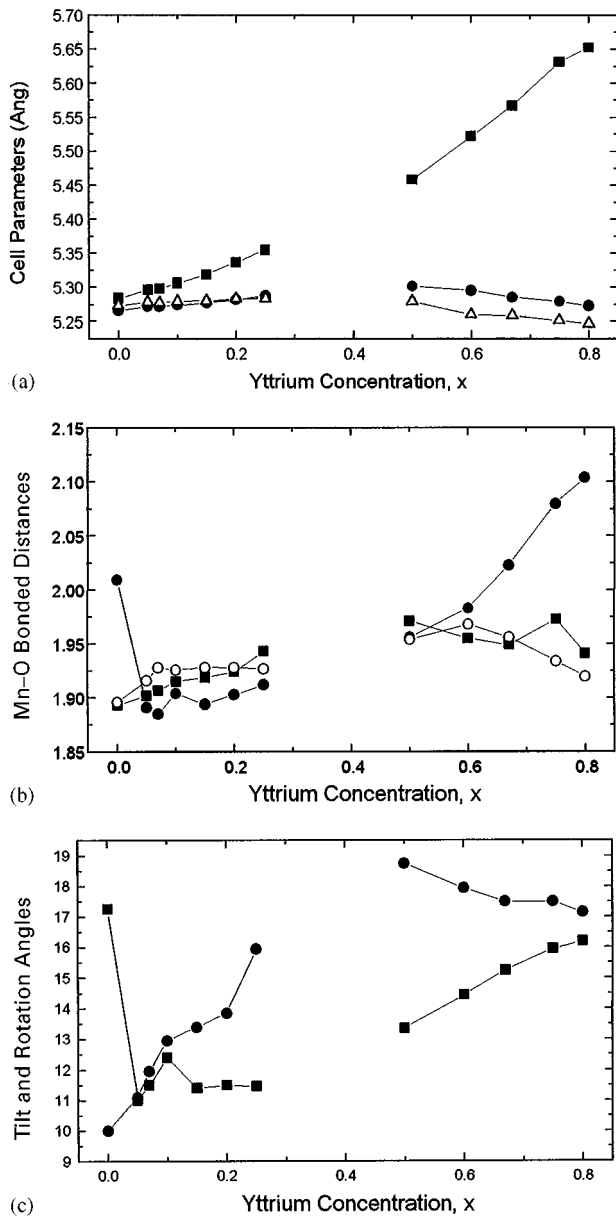


**FIG. 4.** (a) Cell parameters of  $\text{Ca}_{1-x}\text{Y}_x\text{MnO}_3$ . ( $a$ , solid square;  $c$ , solid circle, and  $b/\sqrt{2}$ , open triangle). From yttrium concentration 0.25 to 0.5 orthorhombic O and O' phases coexist. From yttrium content 0.75 to 1 a segregation of the hexagonal  $\text{YMnO}_3$  phase occurs. (b) Mn-O bond distances (Mn-O1, solid square, Mn-O2, solid circle, and Mn-O22, open circle). (c) Tilt and rotation angles of the octahedron ( $\varphi$  tilt angle, solid circle;  $\omega$ , rotation angle, solid square).

to the structure in this kind of materials (2). Therefore, it is necessary to establish whether the samples are really monophasic. While other authors have found a solid solution extending from  $x = 0$  to  $x \sim 0.75$  (4,8) we have found at room temperature a gap in the miscibility between  $x = 0.25$  and  $x = 0.5$ . Two different orthorhombic phases, O

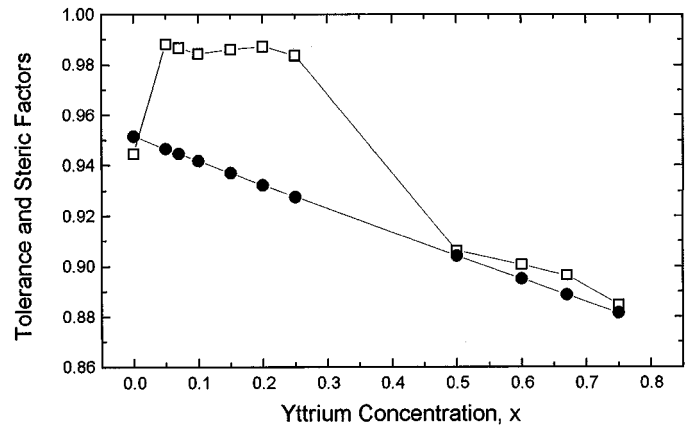


**FIG. 5.** Tolerance and Steric factors as function of yttrium nominal content. (tolerance factor, solid circle; steric factor, open square).

for  $0 \leq x \leq 0.25$  with a 12 coordinated A site and O' for  $0.5 \leq x \leq 0.75$  with a 9 coordinated A site. No phase transition between them occurs. Our results are in

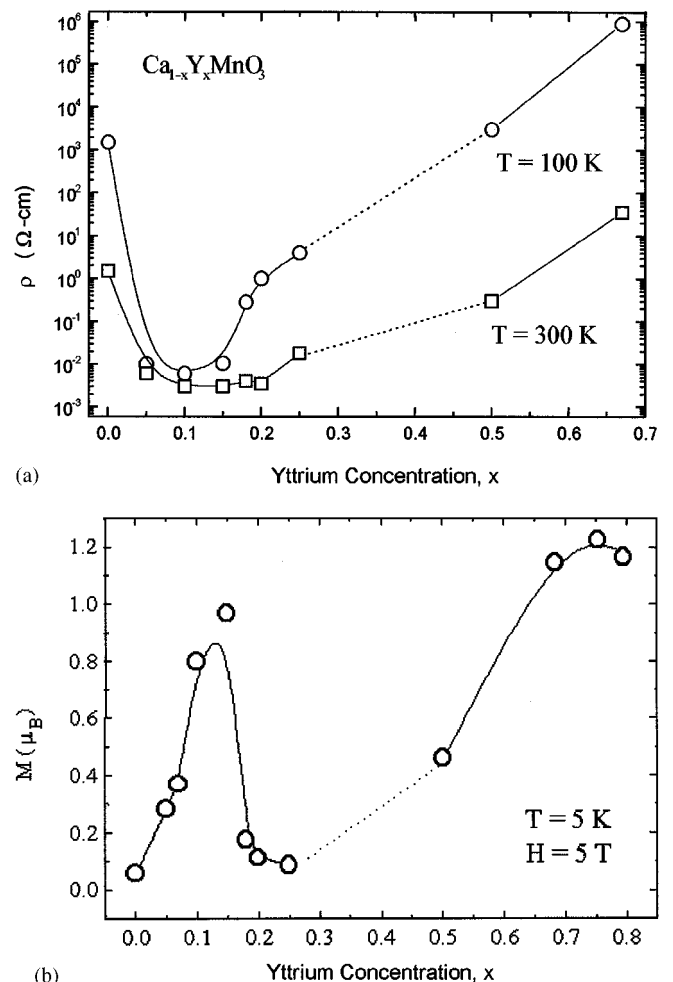


**FIG. 6.** (a)  $\rho$  vs  $x$  for  $T = 100$  and 300 K. (b)  $M$  vs  $x$  measured at  $T = 5$  K and magnetic field  $H = 5$  T.

disagreement with those of Moure *et al.* (9) in the region  $0.6 < x < 1$ , who claimed for the existence of a phase transition orthorhombic–hexagonal at  $x = 0.78$ . As already mentioned, for  $x > 0.8$ , two phases coexist, the hexagonal  $\text{YMnO}_3$  (density =  $5.16 \text{ g/cm}^3$ ) and the orthorhombic  $\text{Ca}_{0.75}\text{Y}_{0.25}\text{MnO}_3$  one (density =  $5.45 \text{ g/cm}^3$ ). The XRD diagram of Moure's paper (9) (see Fig. 2) can be interpreted in terms of our phase diagram as a mixture of hexagonal and orthorhombic phases. No sign of  $2\theta$  displacement of any of the three characteristic hexagonal peaks ( $2\theta \sim 30^\circ$ ) and the characteristic orthorhombic peak at  $2\theta = 26^\circ$  can be observed for their  $x = 0.8$  sample. Besides, their Fig. 3 agrees with a calculated density of a mixture of hexagonal  $\text{YMnO}_3$  and orthorhombic  $\text{Ca}_{1-x}\text{Y}_x\text{MnO}_3$ .

Measured magnetic and transport behaviors shown in Fig. 6 are compatible with our model where two well-differentiated region of Y concentration with different structural properties are present. For low Y concentrations (O-phase samples) we found values  $s \approx 1$  for the steric factor. In this case the measured magnetic and electric behaviors are in agreement with the findings in the well studied series  $\text{Ca}_{1-x}\text{La}_x\text{MnO}_3$ . Therefore, effects associated to the smaller ionic radius of Y are not visible in this low doping region. On the contrary, for high  $x$  (O'-phase) the steric factor is much lower and the compounds are highly distorted because of the small ionic radius of Y and of the Y-Ca radii mismatch. As in Mn perovskites the electrical transport is dominated by the DE interactions, the parameter that describes the hopping process depends on the Mn–O–Mn angle, and the mechanism is more effective when the angle is close to  $180^\circ$ . As it is shown in Fig. 4c,  $\omega$  and  $\varphi$  increase with  $x$ , giving Mn–O–Mn  $\approx 148^\circ$  (for O = O<sub>2</sub>) and  $146^\circ$  (for O = O<sub>1</sub>) in the region  $x \geq 0.5$ . In this case the double-exchange process seems not to be important and as a consequence, a ferromagnetic–metallic state is not found and the resistivity values remain high.

## ACKNOWLEDGMENTS

We acknowledge technical assistance of A. Petragalli, partial support from ANPCYT-Argentina (PICT 3-52-1027) and CONICET-Argentina (H.A. Ph.D. fellowship).

## REFERENCES

1. K. R. Poeppelmeier, M. E. Leonowicz, J. C. Scanlon, J. M. Longo, and W. B. Yelon, *J. Solid State Chem.* **45**, 71 (1982).
2. A. P. Ramirez, *J. Phys. Condens. Matter* **9**, 8171 (1997).
3. Y. Tokura and Y. Tomioka, *J. Mag. Mag. Mater.* **1**, 200 (1999) and references therein.
4. Y. Takeda, Y. Hoshino, Y. Sakaki, T. Kwahara, N. Imanishi, and O. Yamamoto, *J. Mater. Science Lett.* **11**, 1113 (1992).
5. A. Arulraj, R. Gundakaram, A. Biswas, N. Gayathri, A. K. Raychaudhuri, and C. N. Rao, *J. Phys. Cond. Matter* **10**, 4447 (1998).
6. A. Arulraj, P. N. Santhosh, R. Srinivasa Golapan, A. Guha, A. Raychaudhuri, N. Kumar, and C. N. Rao, *J. Phys. Cond. Matter.* **10**, 8497 (1998).
7. P. N. Santhosh, A. Arulraj, P. V. Vanitha, R. S. Singh, K. Sooryanarayana, and C. N. Rao, *J. Phys. Cond. Matter* **11**, L27 (1999).
8. E. Pollert, S. Krupicka, and E. Kuzmicova, *J. Phys. Chem. Solids* **43**, 1137 (1982).
9. C. Moure, M. Villegas, J. F. Fernandez, J. Tartaj, and P. Duran, *J. Mater. Sc.* **34**, 2565 (1999).
10. H. L. Yakel, W. D. Koehler, E. F. Bertaut, and F. Forrat, *Acta Crystallogr.* **16**, 957 (1963).
11. H. Yakel, *Acta Crystallogr.* **8**, 394 (1955).
12. J. Rodriguez-Carbajal, *Physica B* **192**, 55 (1993).
13. M. T. Causa, M. Tovar, A. Caneiro, F. Prado, G. Ibañez, C. A. Ramos, A. Butera, B. Alascio, X. Obradors, S. Piñol, Y. Tokura, and S. B. Oseroff, *Phys. Rev. B* **58**, 3233 (1998).
14. J. Briático, B. Alascio, R. Allub, A. Butera, A. Caneiro, M. T. Causa, and M. Tovar, *Phys. Rev. B* **53**, 14020 (1996).
15. J. Briático, B. Alascio, R. Allub, A. Butera, A. Caneiro, M. T. Causa, and M. Tovar, *Czech. J. Phys.* **46**(S4), 2013 (1996).
16. V. M. Goldschmidt, *Naturwissenschaften* **14**, 477 (1926)
17. R. D. Shannon, *Acta Crystallogr. A* **32**, 751 (1976).
18. C. Martin, A. Maignan, M. Hevieu, and B. Raveau, *Phys. Rev. B* **60**, 12191 (1999).
19. H. Aliaga, M. T. Causa, B. Alascio, H. Salva, and M. Tovar, *J. Mag. Mater.*, in press.